Pergamon

Geochimica et Cosmochimica Acta, Vol. 65, No. 16, pp. 2669–2676, 2001

0016-7037/01 $20.00 + .00

PII S0016-7037(00)00628-7

Strontium heterogeneity and speciation in coral aragonite: Implications for the strontium paleothermometer

N. ALLISON,[1] A. A. FINCH,[2,*] S. R. SUTTON,[3,4] and M. NEWVILLE[4]

[1]Department of Pharmacy and Biomolecular Sciences, University of Brighton, Moulsecoomb, Brighton BN2 4JG, UK
[2]School of Geography and Geosciences and Centre for Advanced Materials, University of St. Andrews, St. Andrews, Fife KY16 9AL, UK
[3]Department of Geophysical Sciences, University of Chicago, Chicago, IL 60637, USA
[4]Consortium for Advanced Radiation Sources, University of Chicago, Chicago, IL 60637, USA

(*Received October* 26, 2000; *accepted in revised form March* 6, 2001)

Abstract—Sea surface temperatures (SSTs) have been inferred previously from the Sr/Ca ratios of coral aragonite. However, microanalytical studies have indicated that Sr in some coral skeletons is more heterogeneously distributed than expected from SST data. Strontium may exist in two skeletal phases, as Sr substituted for Ca in aragonite and as separate $SrCO_3$ (strontianite) domains. Variations in the size, quantity, or both of these domains may account for small-scale Sr heterogeneity. Here, we use synchrotron X-ray fluorescence to map Sr/Ca variations in a *Porites lobata* skeleton at a 5 μm scale. Variations are large and unrelated to changes in local seawater temperature or composition. Selected area extended X-ray absorption fine structure (EXAFS) spectroscopy of low- and high-Sr areas indicates that Sr is present as a substitute ion in aragonite i.e., domains of Sr carbonate (strontianite) are absent or in minor abundance. Variations in strontianite abundance are not responsible for the Sr/Ca fluctuations observed in this sample. The Sr microdistribution is systematic and appears to correlate with the crystalline fabric of the coral skeleton, suggesting Sr heterogeneity may reflect nonequilibrium calcification processes. Nonequilibrium incorporation of Sr complicates the interpretation of Sr/Ca ratios in terms of SST, particularly in attempts to extend the temporal resolution of the technique. The micro-EXAFS technique may prove to be valuable, allowing the selection of coral microvolumes for Sr/Ca measurement where strontium is incorporated in a known structural environment.

1. INTRODUCTION

The substitution of Sr for Ca in aragonite is temperature dependent, and it is possible to use Sr/Ca ratios in coral aragonite as an indicator of local sea surface temperatures (SST; Beck et al., 1992; Evans et al., 1998). The analysis of coralline Sr/Ca has the potential to extend the instrumental record of past SSTs and therefore improve our understanding of climate variability over a range of time scales, including decadal rises in SST and the frequency of El Niño/La Niña events.

However, not all corals exhibit the expected Sr/seawater temperature relationship, and microanalytical studies have indicated that Sr in some coral skeletons is more heterogeneously distributed than expected from SST data (Allison, 1996; Hart and Cohen, 1996). The Sr concentration of coral skeletons (~7000 ppm) exceeds the thermodynamic solubility of Sr in aragonite and Sr may exist in at least two phases: as Sr-substituted for Ca in aragonite, and as separate $SrCO_3$ (strontianite) domains (Greegor et al., 1997). Variations in the size, quantity, or both of these domains may account for small-scale Sr heterogeneity and may explain the departure of some corals from the expected Sr-temperature relationship.

The development of synchrotron radiation techniques allows the determination of both Sr heterogeneity (at a micron scale) and local structural state in materials. Here, we report the in situ application of the X-ray microprobe (5 μm resolution) by synchrotron X-ray fluorescence (SXRF) to map Sr/Ca variations in a *Porites lobata* skeleton and extended X-ray absorption fine structure (EXAFS) spectroscopy to ascertain Sr speciation.

* Author to whom correspondence should be addressed (aaf1@st-and.ac.uk).

2. METHODS

2.1. Samples

Analyses were performed on a *P. lobata* skeleton collected from Tarawa Atoll, Western Pacific (1° N, 172° E) by Dr. Glen Shen. *P. lobata* is probably the most commonly used coral species in paleoenvironmental reconstruction. The core was collected in 1990. An X-radiograph of the core indicated that the material studied here was deposited in approximately 1939 (assuming that high- and low-density band couplets are annual). The oxygen isotope record of this coral is discussed in Cole et al. (1993). The coral material was fixed in epoxy resin, mounted on a pure fused quartz slide (Heraeus Silica and Metals Ltd.) and ground to a thickness of ~15 μm.

2.2. Synchrotron X-ray Fluorescence Microprobe

X-ray fluorescence (XRF) is an analytical method whereby an incident X-ray beam causes excitation of the sample and the emission of characteristic, secondary X-rays (fluorescence). XRF is well understood and widely used to determine composition to the level of parts per million in a variety of materials. SXRF differs from conventional XRF only in that the primary X-ray source is a synchrotron; in all other aspects, the method is analogous. In a synchrotron, charged particles (electrons) move at the speed of light in a circular vacuum chamber, and as they are accelerated through the bending magnet and insertion device components of the accelerator, photons are emitted in highly collimated and intense beams. In a high-energy synchrotron with electron beams at several GeV, the emitted photons have energies in X-ray regime of the electromagnetic spectrum. SXRF has three key benefits over traditional XRF: the intensity of the X-ray beam is many orders of magnitude greater than that from a conventional X-ray generator; the

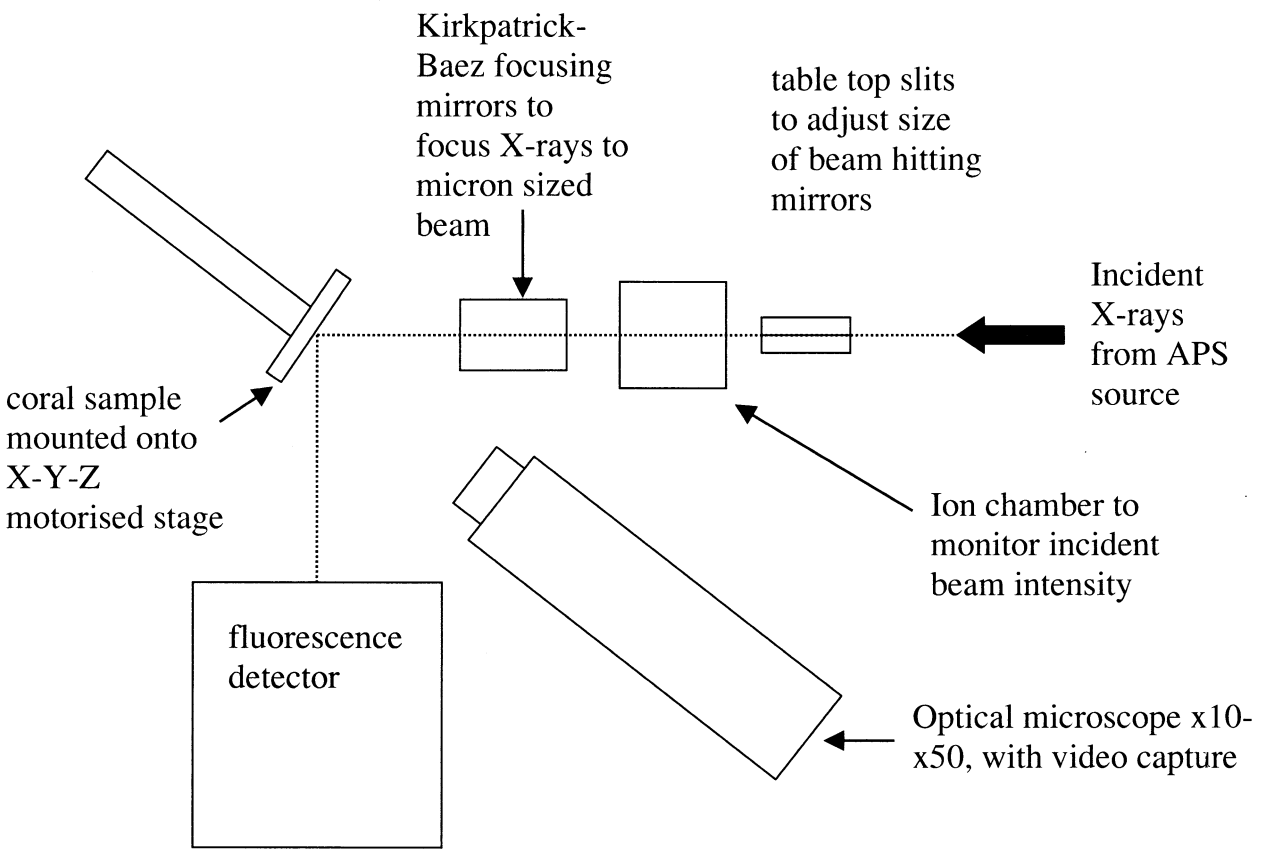

Fig. 1. A schematic diagram of the experimental setup. The coral thin section is mounted onto a motorized stage and moved in steps across the X-ray beam. An optical microscope allows the section to be viewed during the analysis.

X-rays can be focused into a small (at the micron level), intense beam; and monochromators can be used to select the optimum X-ray energy for a particular experiment.

SXRF and EXAFS measurements were carried out with the X-ray microprobe (Smith and Rivers, 1995; Sutton et al., 1995; Sutton and Rivers, 1999) at the Advanced Photon Source (APS), GeoSoilEnviro-CARS Sector 13 (Newville et al., 1999a), Argonne National Laboratory, Illinois, USA. A schematic diagram of the experimental setup is shown in Figure 1. An APS undulator was the X-ray source with a Si(220) channel-cut monochromator used to tune the energy of the incident X-ray beam. For elemental mapping, a monochromatic energy of 16.17 keV was chosen to straddle the Sr K absorption edge to ensure that Sr fluorescence did not saturate the detector. For XAFS spectra, the monochromator and undulator were scanned in unison to keep the energy of the peak of the undulator third harmonic in the Bragg condition defined by the silicon crystal angle. The incident X-ray beam was focused with a novel Kirkpatrick-Baez microfocusing mirror assembly (Eng et al., 1995, 1998; Yang et al., 1995). The Kirkpatrick-Baez mirrors have the advantages of achromaticity (all energies are focused to the same spot), high flux density gains, and long working distances (centimeters) to accommodate an array of ancillary instruments (microscopes, detectors, etc.). The Kirkpatrick-Baez system consisted of two mirrors (100 mm length), one in the horizontal plane and one in the vertical plane, which focused the X-ray beam from 350 μm down to 3×4 μm (flux density gain of $\sim 10^4$ photons s^{-1} μm^{-2}). The mirrors were float glass coated with $\sim$700 Å of Rh. The flat surfaces were dynamically bent to elliptical shapes by use of a mechanical bender. This "double-bounce" focusing system provides excellent harmonic rejection capabilities for EXAFS applications.

The sample was mounted on a motorized stage at 45° to the incident X-ray beam and to the detector (detector at 90° to incident beam and within the horizontal plane of the synchrotron). The beam was scanned at steps of 5 μm each with a residence time of 8 s over an area of 410×200 μm of the thin section. The depth of each analysis was $\sim$20 μm (see below). The core X-radiograph indicated that the linear extension rate of the skeleton was $\sim$12 mm yr^{-1} at the time the material studied here was deposited. An analytical spatial resolution of 20 μm is nominally equivalent to less than 1 day's skeletal growth. Ca and Sr X-ray emissions were measured simultaneously by a 13-element Ge fluorescence detector with energy windows from 3.47 to 3.84 keV (Ca K_α) and from 13.78 to 14.40 keV (Sr K_α), respectively. Two ionization chambers (100 mm, nitrogen) were used for normalization, one upstream of the mirrors (I_0) and one downstream of the sample (I_1). The signal from I_0 was used to normalize the counts in each pixel of the map and each energy step in the XAFS scans.

The efficiency of X-ray emission from the sample is dependent on the sample composition, density, its effective thickness (a product of thickness and porosity), the incident beam energy and the emitted fluorescence energy. All estimates of XRF sensitivity were made by the NRLXRF program (Criss, 1977).

The thickness of coral material in a thin section can be highly variable. *Porites* are perforate corals, and the skeletal structure can be basically described as a series of vertical rods linked by horizontal rungs (Barnes and Lough, 1996). A polished thin section contains areas where the coral fills the depth of the section, voids filled by epoxy resin, and areas where both coral and epoxy resin occur. To minimize errors in Sr/Ca due to thickness variations, we limited our final calculation of Sr/Ca values to points where aragonite appeared to fill the depth of the thin section (as determined by petrographic viewing from front and back of section) and to a narrow range of Ca counts (and therefore a narrow range in effective sample thickness). The typical reduction of beam intensity (I_0/I_1) with the beam on the coral (compared with off the coral) was 19% and is consistent with an analytical depth of $\sim$20 μm of aragonite (ρ = 2.94 g cm^{-3}). The primary beam encounters the

sample at 45° (Fig. 1), and an analytical depth of this value is consistent with a thin section depth of 15 μm. Thus, the effective sample thickness was calculated at each pixel from Ca counts, assuming that Ca was homogeneously distributed throughout the sample and that the maximum counts in the restricted Ca count range equated with the maximum sample depth of 20 μm. In this way, the effective coral thickness was determined to vary from 16 to 20 μm.

To estimate the maximum contributions of background counts from the epoxy resin and the silica slide, analyses were completed on spots where coral filled the depth of the section, where epoxy resin filled the depth of the section, and on an area of the silica slide containing no coral and no epoxy resin. Multiple analyses indicated that Sr and Ca were homogeneously distributed throughout the epoxy resin and silica slide. Ca and Sr counts from the silica slide were 0.3 and 11%, respectively, of counts on the coral. These are overestimates of the potential contamination because during coral mapping, the silica slide is overlain by 16 to 20 μm of aragonite that will absorb some of these counts. The efficiency of Ca and Sr emission from the front of the silica slide through 16 to 20 μm of coral will be 22 to 15% and 73 to 67%, respectively. The silica slide therefore has the potential to increase Ca and Sr counts by a maximum of $<$0.1% and 7 to 8%, respectively. The potential Sr background signal was corrected for the reduction in analytical time used when producing the maps (8 s compared to the 10 s used in the spot analyses) and was used to correct all Sr counts for potential background counts from the slide. We have made no correction for Ca counts from the slide.

Ca and Sr counts from the 20 μm depth of epoxy resin were 4 and 2%, respectively, of counts on the 20 μm depth of coral. We estimate that the maximum depth of epoxy contamination on the coral material will be 4 μm, resulting in a potential increase in Ca and Sr counts in the sample of 0.8 and 0.4%, respectively. Once again, this is an overestimate, as emissions from the epoxy resin will be shielded from the detector by the overlying coral material. Because these figures are minimal, we have made no correction for epoxy resin contamination.

2.3. Ion Probe Microanalysis

The coral Sr/Ca ratios were standardized by means of ion probe microanalyses. Analyses were performed on high- and low-Sr areas of the section with a Cameca ims-4f ion probe at the Department of Geology and Geophysics, University of Edinburgh, UK. Allison (1996) outlines the use of ion probe microanalysis for the detection of trace and minor elements in coralline aragonite. The section was gold-coated and analyzed with a $^{16}O^-$ ion beam, accelerated at 14.5 keV, with a beam current of $\sim$7 nA. An energy offset of 75 $\pm$ 20 eV was used, and the spot size was $\sim$10 μm in diameter. Secondary ions were collected at masses ^{48}Ca and ^{88}Sr. Finding suitable standards to calibrate the ion probe has proved difficult. Most carbonate standards are heterogeneous with respect to Sr, making it impossible to ensure an accurate calibration. Despite this difficulty, analytical precision is good, and concentration differences between samples reflect true variations in geochemistry. Relative ion yields were estimated by similar analyses on two carbonate standards, OKA carbonatite (Sr = 12.356 mmol mol^{-1}) and Iceland Spar (Sr = 0.210 mmol mol^{-1}), to provide two independent estimates of absolute Sr/Ca in the coral sample. Estimates from the two standards varied by 5%. We used the average of these (8.69 mmol mol^{-1} in a Sr-rich area) to standardize the SXRF map. A second ion probe analysis on the Sr-poor area of the section gave an average Sr/Ca concentration of 7.54 mmol mol^{-1}, which is in good agreement with the normalized SXRF map (7.53 mmol mol^{-1}, averaged over four points).

2.4. EXAFS Spectroscopy

X-ray absorption spectroscopy is a family of analytical methods that considers the manner in which X-rays are absorbed by materials as a function of X-ray energy. As the energy of an X-ray approaches the ionization energy of a core electron of an atom, a sudden increase in X-ray absorption is seen. This absorption edge corresponds to the X-ray being absorbed and a core electron being promoted out of the atom. This process is sensitive to the bonding environment of the selected element. Above the absorption edge, the absorption coefficient oscillates with energy, giving EXAFS, which is due to the interference between the photoelectron wave emitted from the absorbing atom and the wave back-scattered from neighboring atoms. These EXAFS oscillations can be related to the radial distribution of atoms about an element by a Fourier transform and quantitatively analyzed to give precise measurements of near-neighbor bond distances and coordination number. In this way, EXAFS provides information about the local structural and chemical environment about a particular element. EXAFS measurements can be carried out on a variety of sample environments, from bulk powders to solutions, but as the latest synchrotron sources produce ever brighter X-ray sources, EXAFS spectroscopy on small areas (down to a few microns) within heterogeneous samples has become feasible.

EXAFS measurements were made with a 5 μm diameter X-ray beam on individual spots corresponding to Sr-high and Sr-low areas, identified from the SXRF maps. The monochromatic X-ray beam was scanned across the Sr K absorption edge between 16.08 and 16.40 keV at 1.5eV intervals, with a 2 s residence time per point. The Sr K_α fluorescence region (13.78–14.40 keV) in 8 of the 13 detector elements was used for the EXAFS, and eight successive scans were summed for the EXAFS spectra reported here.

3. RESULTS

3.1. Calcium and Strontium Microdistributions

The Ca K_α image (Fig. 2a) shows large variations, reflecting the transition from epoxy-filled voids (very low Ca semicircular regions) to coral (high Ca). The image is dominated by a large area of nearly uniform intensity (lower two-thirds of image), two epoxy-filled voids (top right and top left-center), a small high count region (top center), and slightly reduced horizontal zone (middle) interpreted as a zone of slightly lower effective thickness. The strontium K_α image (Fig. 2b) has a pronounced lobelike structure in addition to the features observed in Figure 2a. There is no obvious correlation between the microdistributions of Ca and Sr in the coral-bearing regions of the maps.

Sr/Ca ratios were calculated at each pixel in the map. Because of the uniformity of the Ca image, the Sr/Ca microdistribution (Fig. 2c) is broadly similar to that of Sr alone, although new features associated with the voids in the section are now apparent. Note in particular that the horizontal band (middle), apparent in both the Ca (Fig. 2a) and Sr (Fig. 2b) images, is absent in the Sr/Ca image (Fig. 2c), consistent with a slight variation in effective thickness.

Sr/Ca ratios show a wide variation, from 0.65 to 3.15, across the image. The lowest Sr/Ca ratios occur to the right of the central void, whereas the highest ratios occur to the left of both voids. To interpret more fully the Sr/Ca distribution, the relationships between Ca counts and Sr/Ca ratio are shown in histogram form (Fig. 3). The histogram for Ca K_α (Fig. 3a) indicates that the majority of the pixels (85%) lie in a narrow distribution between 22,000 and 25,000 counts (denoted region **Y**). The remaining pixels can be divided into two regions: **X** (0–22,000 counts, 11% of the pixels) where there are counts lower than the median region, and **Z** (25,000–33,000 counts, 4% of the pixels), where there are high counts.

We examined the Sr/Ca distributions of all points together (Fig. 3b) and in each region of the Ca distribution separately (Figs. 3c–e). High Ca counts (region **Z**, center top of Fig. 2a) produce relatively low Sr/Ca ratios (Fig. 3e). We interpret this to be an artefact due to the proximity of the region to the epoxy-filled void (Fig. 2c). In Figure 2, the X-ray beam enters the sample from the right with a 45° inclination to the plane of

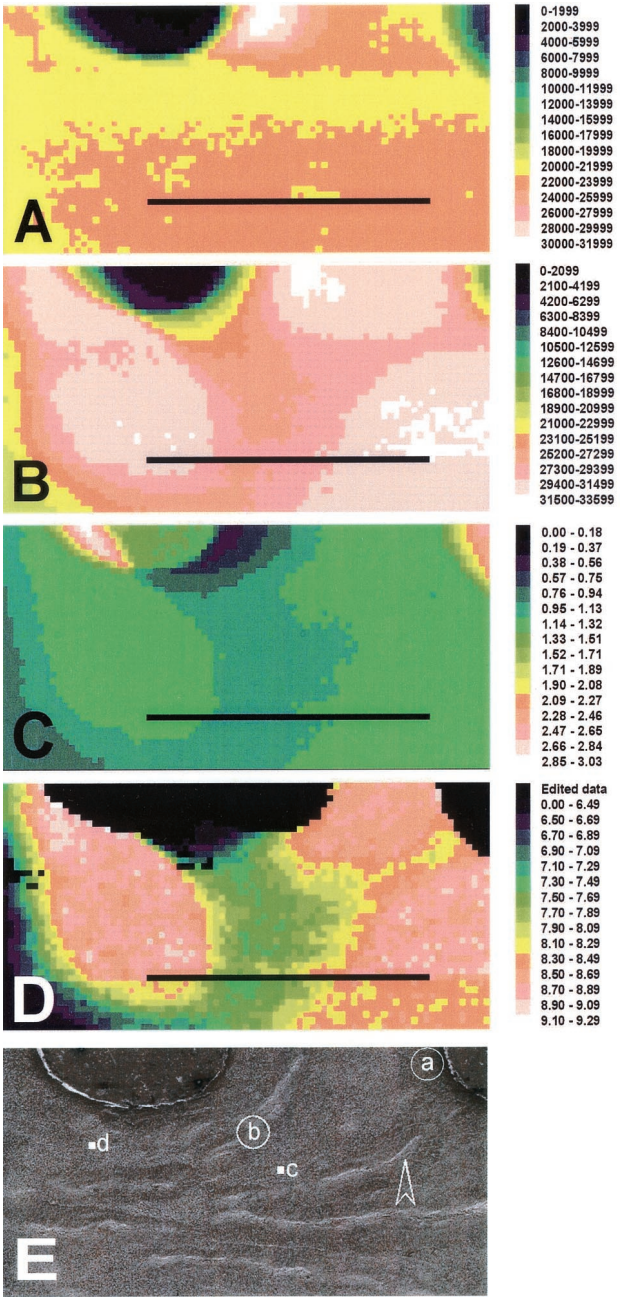

Fig. 2. Microdistribution images (410 × 200 μm area) of (a) Ca counts, (b) Sr counts, and (c) Sr/Ca ratios for the full data set. The color scheme is chosen to grade from black through cold colors (blue and green) to warmer colors (orange and red) to white (hot). The dark strip across the bottom section of each image indicates a portion of the scan when no X-rays were delivered. These strips are useful registry markers and internal scale bars because they are exactly 5 × 220 μm. (d) Calculated Sr/Ca ratios across the coral thin section for the filtered data set (see text). The color bar at the right of the image has units of mmol mol^{-1}. (e) SEM micrograph of the mapped area after a 0.1 M HCl etch. Centers of calcification, from which crystal growth begins, are visible as slight hollows on the coral surface (indicated by the arrow). High- and low-Sr areas analyzed by ion probe microanalysis for standardization are marked a and b, respectively. Low- and high-Sr areas analyzed by EXAFS are marked c and d, respectively.

the page. The detector viewing direction is from the left, with a 45° inclination to the plane of the page (90° between the two rays). Fluorescence generated in the coral to the right of the void exits the sample through epoxy rather than through coral, and the absorption contrast between these two materials results in an enhanced fluorescence signal. As Ca K_α X-rays are of a lower energy than those of Sr K_α, this effect has a greater influence on Ca counts. We estimate that the maximum enhancement, produced when the epoxy–coral interface plane contains the incoming beam, is ~30 and 6% for Ca and Sr, respectively, values close to those observed.

Low Ca values (region **X**) are responsible for a wide spread of Sr/Ca ratios including very large values in the overall distribution (Fig. 3c). These pixels occur to the left of the void (Fig. 2c). Here, the primary X-ray beam penetrates the epoxy-filled void before encountering coral toward the back of the sample. X-rays generated at the back of the sample reach the detector through the thickness of the section, and are partly absorbed. Because Ca K_α X-rays are of a lower energy than Sr K_α, the former are absorbed more, resulting in an increased Sr/Ca ratio. This region also represents an artefact associated with the void.

The Sr/Ca ratios for region **Y** (the majority of the pixels) have a relatively narrow distribution (Fig. 3d). These points represent coral material that fills the thickness of the analytical depth and in which artefacts caused by proximity to voids are absent. This is confirmed by visual examination of the section. To overcome difficulties caused by artefacts associated with the voids, we restrict our estimates of absolute Sr/Ca to the points defined by region **Y**. Sr/Ca count ratios in Figure 2c were converted to estimates of absolute concentration by standardization against ion probe microanalysis, after pixels corresponding to regions **X** and **Z** were edited from the data set (Fig. 2d). Sr/Ca variations in the section are up to 3.5 mmol mol^{-1}. The distribution of Sr is systematic, with Sr concentrated in certain areas (e.g., the lobe-shaped area on the left hand side of the slide).

3.2. Correlations between Chemical Microdistributions and Skeletal Structure

In an attempt to relate this Sr heterogeneity to skeletal structure, the thin section was etched briefly in 0.1 mol/L HCl to enhance structure, sputter-coated with gold, and viewed with a JEOL JSM-6000 scanning electron microscopy (SEM; Fig. 2e). The locations of the ion probe and EXAFS microanalyses are marked on this micrograph.

The micrograph indicates that the crystallites in the section are arranged in radiating, nonrandom directions, and differential diffraction effects may occur between pixels in the maps. However, diffraction effects would be manifest as sympathetic changes in Ca and Sr counts. Ca counts show little variation over the regions of the section used in the calculation of Sr/Ca values (region **Y**), indicating that diffraction does not vary significantly over this area. In addition, our measured thickness of the section is in good agreement with our estimated value from I_1/I_0, indicating that little X-ray energy is dissipated in diffraction.

The centers of calcification (the origins of crystal growth, indicated with an arrow in Fig. 2e) are visible as discontinuous

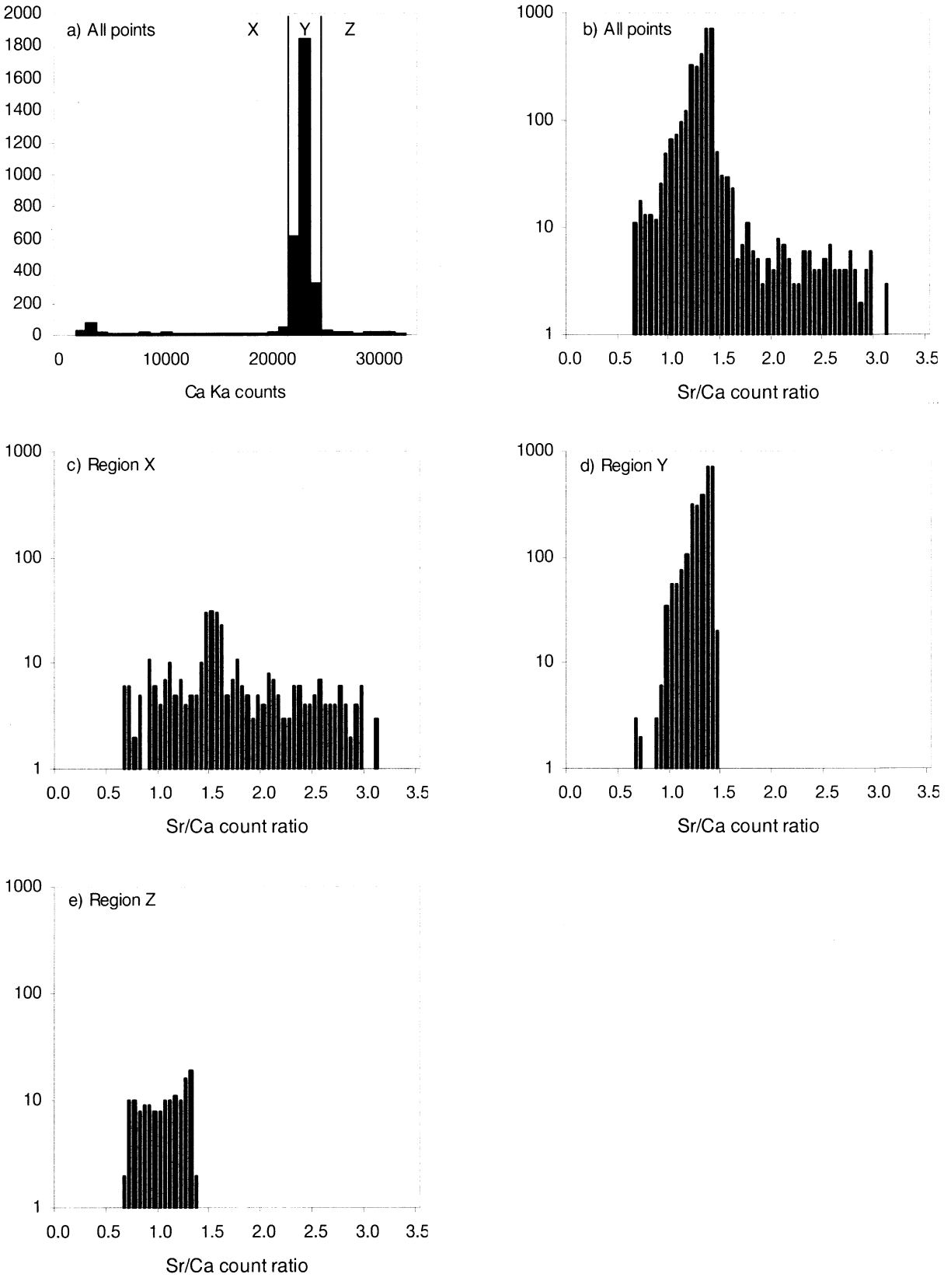

Fig. 3. Histograms of pixel values from the SXRF maps in Figure 2. (a) Distribution of calcium K_α counts divided into three main regions labeled **X**, **Y**, and **Z** (see text). The remaining four histograms show the distributions of Sr/Ca ratio for the full map (b) and the four calcium regions (c–e) indicated in (a).

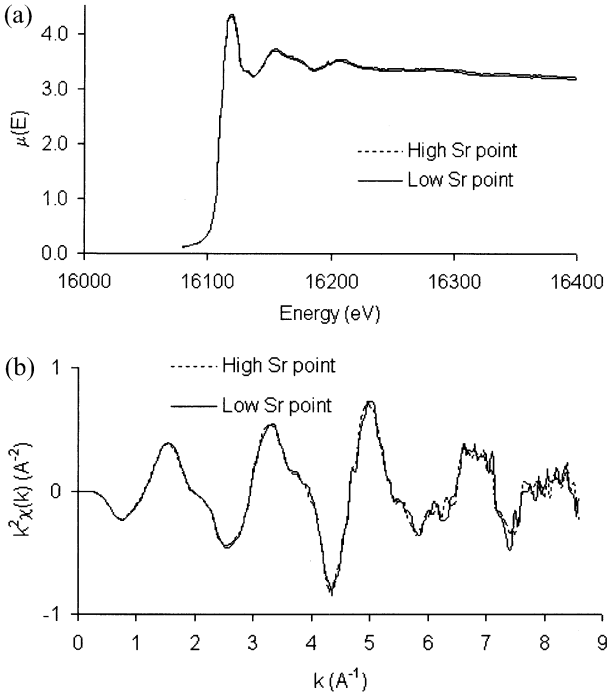

Fig. 4. Strontium K-edge X-ray absorption spectra for Sr in coral. (a) Raw absorption spectra, μ(E), for two successive measurements. (b) Isolated fine structure, $k^2\chi$(k), for the same two measurements.

white lines running across the photograph. Centers of calcification contain less aragonite by volume (Wainwright, 1964) and appear as hollows by SEM, suggesting that these areas have a higher degree of microporosity than the surrounding skeletal areas. The efficiency of X-ray emission from the sample may be affected by variations in sample porosity. However, there is no indication that these small changes in porosity, associated with centers of calcification, affect the determinations of Sr/Ca variations in this sample. However, the Sr microdistribution does appear to correlate with the crystalline fabric of the coral skeleton. The low- and high- Sr regions identified in Figure 2e correspond with different centers of calcification.

3.3. Strontium Structural State

Strontium K-edge micro-EXAFS spectra (Fig. 4) were collected from one Sr-low and one Sr-high region of the thin section (points c and d, respectively; Fig. 2e). Fourier transforms of the EXAFS oscillations (Fig. 5, with the EXAFS weighted by k^2) show peaks corresponding to the Sr near neighbors. Note that the peaks in the EXAFS Fourier transform are shifted from the interatomic distances by ~0.5 Å, the result of well-understood phase shifts of the scattering photoelectron. The graphs show no discernible difference for Sr-rich and Sr-poor areas of the coral aragonite, indicating that Sr is in the same structural state in both spots. The data are in good agreement with an *ab initio* calculation (by FEFF version 7.0; Zabinsky et al., 1995) of the EXAFS spectrum for Sr substituted for a single Ca atom in aragonite (with a Sr-Ca distance around 3.8 Å) and in poor agreement with measured Sr K-edge

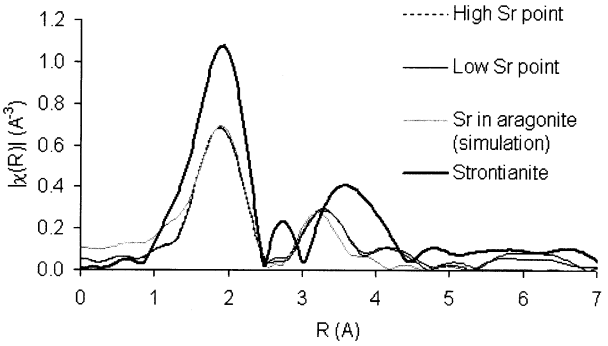

Fig. 5. Fourier transforms (weighted by k^2) of the EXAFS in Figure 4b, corresponding to the average radial distribution of atoms around Sr. The peaks in the EXAFS Fourier transform are shifted from the interatomic distances by ~0.5 Å because of phase shifts of the scattering photoelectron. Shown are two nearly identical measurements of Sr in coral, a measurement of Sr in strontianite, and a simulation of Sr substituted for Ca in aragonite. Although the first shells are similar for all spectra (corresponding to Sr-O at ~2.5 Å), the differences in the peaks between 3 and 4 Å clearly show the Sr in coral to be more consistent with Ca third neighbors of the aragonite structure than with Sr third neighbors of the strontianite structure.

EXAFS (Newville et al., 1999b) of strontianite, with a Sr-Sr distance of 4.2 Å (Fig. 5).

4. DISCUSSION

Sr/Ca variations across the section are large (Fig. 2d), up to 2.7 mmol mol^{-1}, which is equivalent to an apparent seawater temperature change of ~34°C on the *Porites* paleothermometer (de Villiers et al., 1994). Hart and Cohen (1996) and Allison (1996) both report large Sr/Ca variations (up to 0.6 mmol mol^{-1}) over small skeletal distances (nominally equivalent to less than 1 week's growth). The larger variations reported here may reflect the finer spatial resolution of the technique used in the present study.

The mean Sr/Ca ratio of our sample map (8.26 mmol mol^{-1}) is equivalent to 34°C on the *Porites* paleothermometer (de Villiers et al., 1994). This ratio is 6% lower than the Sr/Ca value (8.69 mmol mol^{-1}) expected from the average annual seawater temperature of 28.5°C (Shen and Dunbar, 1995). At least part of this discrepancy may be due to uncertainties in the ion probe calibration. Multiple analyses of carbonate samples and standards indicate that calibration uncertainties may introduce an error of up to 10% on Sr/Ca determinations in coral (Allison, 1996). This alone is sufficient to account for the discrepancy between the observed and expected mean Sr/Ca. Analytical precision of ion probe microanalyses is good (<1%), and the relative concentration differences between samples reflect true variations in geochemistry. Although it is possible that our calibration of the SXRF map has resulted in a small systematic underestimate of the true Sr/Ca values, the Sr/Ca variations are real. However, the median in the Sr/Ca histogram (Fig. 3d) corresponds to 8.9 mmol mol^{-1}, within 2.5% of the value expected from the average temperature. It should be emphasized that only a 0.1 mm^2 area has been considered in the present study, and it is possible that the average composition of the area studied is slightly different from that of the bulk of the material.

The Sr/Ca variability is observed over skeletal distances of 150 μm. Linear extension rates of corals in this area are typically 11 mm yr^{-1}, so 150 μm is nominally equivalent to ~5 d of skeletal growth. Although calcification occurs at the coral surface in *Porites*, skeletal thickening may also occur throughout the tissue layer, which usually extends up to several millimeters into the coral skeleton (Barnes and Lough, 1993). It is therefore possible that the low- and high-Sr regions were deposited some time apart. However, the large Sr/Ca variations are far in excess of the annual Sr/Ca variations expected from the annual seawater temperature range of 1.5°C (Levitus, 1982), which equates to a Sr/Ca variation of 0.119 mmol mol^{-1} on the *Porites* paleothermometer. Rainfall in the study area is highly seasonal, and the salinity may vary annually by as much as 4‰ (Levitus, 1982). However, observations at a range of other sites, depths, and salinity imply that the effect of this on seawater Sr/Ca will be relatively small: differences in seawater Sr/Ca of 0.158 mmol mol^{-1} have been reported at sites where salinity varied by up to 1.3‰ (de Villiers et al., 1994).

The Sr/Ca variations are unrelated to changes in local seawater temperature or composition. EXAFS measurements of low- and high-Sr areas indicate that Sr substitutes in aragonite and that domains of Sr carbonate (strontianite) are absent or in minor abundance. This is in contrast to previous reports that inferred domains of strontianite in several coral genera, including *Porites* (Greegor et al., 1997; Pingitore et al., 1997). Our analyses focused on small areas of the coral skeleton, and it is possible that areas containing strontianite were not included in the analyses. However, our results indicate that variations in the chemical speciation of strontium are not responsible for the small-scale Sr heterogeneity observed in this coral. The Sr concentration nominally extends beyond the Sr solubility limit in aragonite, indicating that the coral is precipitating metastable Sr-supersaturated aragonite.

The origin of the variability in the Sr/Ca ratio is at present unresolved. However, the distribution of Sr appears to be systematic. Examination of the analyzed area by SEM indicates that the centers of calcification, which are the origins of crystal growth, are discontinuous and correspond with the low- and high-Sr regions. This suggests that the different regions were deposited as the result of different calcification events.

There are few observations of calcification processes in the massive coral species usually used for paleoenvironmental reconstruction. However, detailed observations of calcification processes in branching coral species indicate that more than one mechanism of calcification may occur. Calcification follows a pattern with diurnal variations in calcification rate (Barnes and Chalker, 1990), skeletal extension rate (Barnes and Crossland, 1982; Strömgren 1987), crystal habit (or shape) (Gladfelter, 1983; le Tissier, 1988; Hidaka, 1991), and deposition site (Marshall and Wright, 1998). The high and low Sr regions observed in this study are too large to represent areas deposited in single days or nights. However, they may represent zones deposited by different calcification processes over different periods. Aragonite formation is a disequilibrium process (Plummer and Busenberg, 1987; Plummer et al., 1992) that may be strongly mechanism dependent; that is, Sr-bearing aragonite formed by one process may have a wholly different composition to that formed in another manner, under the same pressure and temperature. There is evidence that the Sr/Ca concentration of coral skeletons may be inversely related to skeletal extension rate (de Villiers et al., 1994, 1995), indicating that variations in calcification processes have the potential to affect Sr/Ca content.

Our existing understanding of Sr incorporation in coral aragonite inadequately explains the magnitude of Sr heterogeneity observed here. Strontium heterogeneity may reflect nonequilibrium calcification processes, which will complicate the interpretation of Sr/Ca ratios in terms of SST, particularly in attempts to extend the temporal resolution of the technique. Microbeam techniques have the potential to allow resolution of SSTs on a weekly or even daily scale. However, it may be that extension rate, coupled with yet unknown factors and the juxtapositioning of aragonite of differing ages, wholly dominates the Sr/Ca signal on the small scale. Further work will ascertain the factors that control how Sr/Ca heterogeneity on the small scale is expressed on the large scale. The micro-EXAFS technique may prove to be extremely valuable in the push to higher temporal resolution, allowing the selection of coral microvolumes for Sr/Ca measurement where strontium is incorporated in a known structural environment.

Acknowledgments—This work was supported by the Natural Environment Research Council, UK (N.A.) and the Mineralogical Society of Great Britain and Ireland (N.A.). GeoSoilEnviroCARS is supported by the U.S. National Science Foundation (EAR-9906456) and the U.S. Department of Energy (DE-FG02-94ER14466). Use of the Advanced Photon Source was supported by the U.S. Department of Energy under contract W-31-109-Eng-38. The assistance of John Craven and Richard Hinton (University of Edinburgh) with the SIMS analyses is gratefully acknowledged. We are grateful to Glen Shen, who supplied the coral material. We thank N. Pingitore, Jr., and D. A. Vanko for constructive reviews of this article in manuscript.

Associate editor: M. A. McKibben

REFERENCES

Allison N. (1996) Comparative determinations of trace and minor elements in coral aragonite by ion microprobe analysis, with preliminary results from Phuket, South Thailand. *Geochim. Cosmochim. Acta* **60,** 3457–3470.

Barnes D. J. and Crossland C. J. (1982) Variability in the calcification rates of *Acropora acuminata* measured by radioisotopes. *Coral Reefs* **1,** 53–57.

Barnes D. J. and Chalker B. E. (1990) Calcification and photosynthesis in reef-building corals and algae. In *Coral Reefs* (ed. Z. Dubinsky), pp 109–131. Elsevier.

Barnes D. J. and Lough J. M. (1993) On the nature and causes of density banding in massive coral skeletons. *J. Exp. Mar. Biol. Ecol.* **167,** 91–108.

Barnes D. J. and Lough J. M. (1996) Coral skeletons: Storage and recovery of environmental information. *Global Change Biol.* **2,** 569–582.

Beck J. W., Edwards R. L., Ito E., Taylor F. W., Recy J., Rougerie F., Joannot P., and Henin C. (1992) Sea surface temperature from coral skeletal strontium/calcium ratios. *Science* **257,** 644–647.

Cole J. E., Fairbanks R. G., and Shen G. T. (1993) Recent variability in the Southern Oscillation—Isotopic results from a Tarawa atoll coral. *Science* **260,** 1790–1793.

Criss J. W. (1977) NRLXRF—Cosmic program DOD-00065. U.S. Naval Research Laboratory.

de Villiers S., Nelson B. K., and Chivas A. R. (1995) Biological controls on coral Sr/Ca and $\delta^{18}O$ reconstructions of sea surface temperatures. *Science* **269,** 1247–1249.

de Villiers S., Shen G. T., and Nelson B. K. (1994) The Sr/Ca-temperature relationship in coralline aragonite: Influence of variabil-

ity in (Sr/Ca) seawater and skeletal growth parameters. *Geochim. Cosmochim. Acta* **58,** 197–208.

Eng P. J., Rivers M. L., Yang B. X. and Schildkamp W. (1995) Microfocusing 4-keV to 65-keV X-rays with bent Kirkpatrick-Baez mirrors. *Proc. SPIE* **2516,** 41–51.

Eng P. J., Newville M., Rivers M. L. and Sutton S. R. (1998) Dynamically figured Kirkpatrick Baez micro-focusing optics. In *X-Ray Microfocusing: Applications and Technique* (ed. I. McNulty). *Proc. SPIE* **3449**, 145.

Evans M. N., Fairbanks R. G., and Rubenstone J. L. (1998) A proxy index of ENSO teleconnections. *Nature* **394,** 732–733.

Gladfelter E. H. (1983) Skeletal development in *Acropora cervicornis* II. Diel patterns of calcium carbonate accretion. *Coral Reefs* **2,** 91–100.

Greegor R. B., Pingitore N. E. Jr., and Lytle F. W. (1997) Strontianite in coral skeletal aragonite. *Science* **275,** 1452–1454.

Hart S. R. and Cohen A. L. (1996) An ion probe study of annual cycles of Sr/Ca and other trace elements in corals. *Geochim. Cosmochim. Acta* **60,** 3075–3084.

Hidaka M. (1991) Deposition of fusiform crystals without apparent diurnal rhythm at the growing edge of septa of the coral *Galaxea fascicularis. Coral Reefs* **10,** 41–45.

le Tissier, M. D. A. (1988) Diurnal patterns of skeleton formation in *Pocillopora damicornis* (Linnaeus). *Coral Reefs* **7**, 81–88.

Levitus S. (1982) *Climatological Atlas of the World.* NOAA Prof. Paper 13. National Oceanic and Atmospheric Administration.

Marshall A. T. and Wright A. (1998) Coral calcification: Autoradiography of a scleractinian coral *Galaxea fascicularis* after incubation in ^{45}Ca and ^{14}C. *Coral Reefs* **17,** 37–47.

Newville M., Sutton S., Eng P. J., and Rivers M. (1999a) Micro-beam XAFS, XRF, and XRD at APS 13-ID. *J. Synchrotron Rad.* **6,** 353–355.

Newville M., Carroll S. A., O'Day P. A., Waychunas G. A., and Ebert M. (1999b) A Web-based library of XAFS data on model compounds. *J. Synchrotron Rad.* **6,** 276–277.

Pingitore N. E. Jr., Greegor R. B., Lytle F. W., and Wellington G. W. (1997) Presence of strontianite documented in additional coral taxa by X-ray absorption spectroscopy. *Eos Trans. AGU* **78(18),** fall supplement.

Plummer L. N. and Busenberg E. (1987) Thermodynamics of aragonite–strontianite solid solutions: Results from stoichiometric solubility at 25 and 76°C. *Geochim. Cosmochim. Acta* **51,** 1393–1411.

Plummer L. N., Busenberg E., Glynn P. D., and Blum A. E. (1992) Dissolution of aragonite–strontianite solid solutions in nonstoichiometric $Sr(HCO_3)_2$-$Ca(HCO_3)_2$-CO_2-H_2O solutions. *Geochim. Cosmochim. Acta* **56,** 3045–3072.

Shen G. T. and Dunbar R. B. (1995) Environmental controls on uranium in reef corals. *Geochim. Cosmochim. Acta* **59,** 2009–2024.

Smith J. V. and Rivers M. L. (1995) Synchrotron X-ray microanalysis. In *Microprobe Techniques in the Earth Sciences*(eds. P. J. Potts, J. F. W. Bowles, S. J. B. Reed, and M. R. Cave), pp. 163–233. Chapman and Hall.

Strömgren T. (1987) The effect of light on the growth rate of intertidal *Acropora pulchra* (Brook) from Phuket, Thailand, lat. 8°N. *Coral Reefs* **6,** 43–47.

Sutton S., Bajt S., Delaney J., Schulze D., and Tokunaga T. (1995) Synchrotron X-ray fluorescence microprobe: Quantification and mapping of mixed valence state samples using Micro-XANES. *Rev. Sci. Instrum.* **66,** 1464–1467.

Sutton S. R. and Rivers M. L. (1999) Hard X-ray synchrotron microprobe techniques and applications. In *CMS Workshop Lectures,*Vol. 9, *Synchrotron Methods in Clay Science* (eds. D. G. Schulze et al.), pp. 146–163. Clay Mineral Society.

Wainwright S. A. (1964) Studies of the mineral phase of coral skeleton. *Exp. Cell Res.* **34,** 213–230.

Yang B. X., Rivers M. L., Schildkamp W., and Eng P. (1995) GeoCARS micro-focusing Kirkpatrick-Baez mirror bender development. *Rev. Sci. Instrum.* **66,** 2278–2280.

Zabinsky S. I., Rehr J. J., Ankudinov A., Albers R. C., and Eller M. J. (1995) Multiple-scattering calculations of X-ray absorption. *Phys. Rev. B* **52,** 2995–3009.